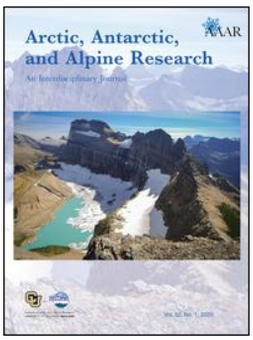

Arctic, Antarctic, and Alpine Research

An Interdisciplinary Journal

ISSN: (Print) (Online) Journal homepage: https://www.tandfonline.com/loi/uaar20

Elevational ground/air thermal gradients in the Swiss inner Alpine Valais

Armin Rist , Lotti Roth & Heinz Veit

To cite this article: Armin Rist , Lotti Roth & Heinz Veit (2020) Elevational ground/air thermal gradients in the Swiss inner Alpine Valais, Arctic, Antarctic, and Alpine Research, 52:1, 341-360, DOI: 10.1080/15230430.2020.1742022

To link to this article: https://doi.org/10.1080/15230430.2020.1742022

ARCTIC, ANTARCTIC, AND ALPINE RESEARCH
2020, VOL. 52, NO. 1, 341–360
https://doi.org/10.1080/15230430.2020.1742022

Elevational ground/air thermal gradients in the Swiss inner Alpine Valais

Armin Rist, Lotti Roth, and Heinz Veit

Institute of Geography, University of Bern, Bern, Switzerland

ABSTRACT

The dependence of air temperature on elevation (i.e., its elevational gradient) in the mountains is well known. However, the elevational gradient of near-surface ground temperatures and derived thermal parameters is much less understood. In this study, we investigated how these parameters depend on elevation by one-year temperature measurements along a transect in the Valais Alps (Switzerland) between 700 and 2,600 m a.s.l. In addition, we studied the effect of differences in slope aspect (north/south) and land cover (open field/forest). Air temperatures were measured as a reference. The results show that the ground thermal regime distinctly differs from that of the air. These differences could mainly be attributed to radiation, snow cover, and ground heat transfer. Our findings have far-reaching implications for ecosystems, agriculture, and forestry in mountains because a large portion of the living biomass is underground and thus affected by ground thermal processes.

ARTICLE HISTORY
Received 5 May 2019
Revised 16 February 2020
Accepted 3 March 2020

KEYWORDS
Ground thermal regime; elevational gradient; slope aspect; land cover; mountains

Introduction

The annual mean of the elevational air temperature gradient—alternatively often called air temperature lapse rate—is defined as −0.65°C/100 m elevational difference for the international standard troposphere (Blüthgen 1980). This gradient is valid for the average free atmosphere with a mixed humid/dry adiabatic elevational gradient. However, for the near-surface atmosphere it can strongly vary in space and time: regarding the spatial variations, the dependence of the elevational T_a gradient on climate has been investigated by, for example, Pepin (2001), Minder, Mote, and Lundquist (2010), and Navarro-Serrano et al. (2018), and its dependence on the relief has been investigated by, for example, Rolland (2003), Tang and Fang (2006), Minder, Mote, and Lundquist (2010), Kirchner et al. (2013), and Cordova et al. (2016). In addition, the temporal variations of the elevational T_a gradient due to subdaily and seasonal temperature cycles were studied intensively by, for example, Bouet (1978), Müller and Whiteman (1988), Fries et al. (2009), and Minder, Mote, and Lundquist (2010).

Though the mean annual air temperature typically shows a linear relation to elevation, this is not necessarily the case for other thermal parameters of the free atmosphere. For example, the number of frost change days increases with elevation up to about 1,400 to 1,700 m due to the elevational temperature decrease, but decreases above because the air temperatures less frequently exceed 0°C (Veit 2002). Thermal air parameters are affected not only by elevation but by other factors such as land cover, snow cover, and aspect.

Compared to air temperatures and related thermal parameters in mountain areas, soil or ground temperatures are rarely studied except when focusing on permafrost (e.g., Zenklusen Mutter, Blanchet, and Phillips 2010). However, ecologically, the near-surface ground temperature and related thermal parameters are crucial (Löffler 2007; Graae et al. 2012). Ground temperatures are especially important in mountainous terrain because the main respiring biomass of most alpine plants is situated in the ground; that is, in the root zone (Körner 2003). Ground and air temperatures might be affected differently by climate change and, consequently, microrefugia for species living predominantly below- or aboveground (Ashcroft and Gollan 2013).

Elevational gradients of the ground temperature and related thermal ground parameters are clearly influenced by the decrease in air temperature with elevation. In addition, the number of ground ice days for which

CONTACT Armin Rist armin.rist@giub.unibe.ch; armin.rist@gmail.com Institute of Geography, University of Bern, Hallerstrasse 12, Bern CH-3012, Switzerland.

Present address for Lotti Roth: ILA Institut für Laufbahn und Arbeit GmbH, Eichenstr. 16, CH-3074 Muri b. Bern, Switzerland.

the maximum daily ground temperature does not exceed 0°C increases with elevation (Lehmkuhl and Klinge 2000). However, thermal ground parameter gradients are strongly modified by further climatic and site-specific factors. The effect of radiation was investigated by, for example, Barry (2008), Maurer (1916), Aulitsky (1962), and Happoldt and Schrott (1989). Grunow (1952), Turner, Rochat, and Streule (1975), and Barry (2008) investigated the effects of slope aspect. The influence of snow cover was studied by, for example, Richter (1996) and Barry (2008). Haberkorn et al. (2017) studied the effects of solar radiation and snow depth on near-surface rock temperatures at the lower limit of alpine permafrost using temperature transects over a steep mountain ridge. Precipitation, water, and ground ice content and how they influence the ground thermal regime were addressed by, for example, Happoldt and Schrott (1989), Richter (1996), Lehmkuhl and Klinge (2000), and Rist (2007). The latter publications also deal with the effect of ground depth on the near-surface ground temperatures. Lehmkuhl and Klinge (2000) reported on frost, ice, and frost change days for different kinds of land cover.

Remote sensing was applied in several studies to determine the spatial distribution of ground surface temperatures at the coarse scale of landscapes (e.g., Zhang, Armstrong, and Smith 2003; Bertoldi et al. 2010; Coppernoll-Houston and Potter 2018). These indirectly determined ground surface temperatures reflect the thermal conditions of the superficial layer of vegetation or bare ground and differ from those within the ground where direct radiation is eliminated.

The near-surface ground thermal regime has not yet been studied systematically by means of a transect of direct measurements in the ground along a north–south-oriented cross section through an alpine valley covered by forest and open fields. The objective of this study is to quantify how temperatures and derived thermal parameters depend on elevation in the near-surface ground in contrast to air. The article additionally seeks to determine the reasons and controls involved. In order to reach these objectives, the following research questions are defined:

- Do temperatures, related thermal parameters, and their elevational gradients in mountains differ between air and near-surface ground, regarding daily and seasonal courses and amplitudes as well as yearly means?
- How do ground and air temperatures and related thermal parameters in mountains depend on the integrative environmental factor elevation, both generally and separated by aspect and land cover as co-factors?
- Which basic physical factors are integrated in and vary by elevation, aspect, and land cover, and how do they ultimately govern the ground thermal regime compared to that of air?

Material and methods

Study site

The study was performed along an elevational cross-profile through the Rhone valley, one of the Alpine main valleys, in the Canton of Valais, western Swiss Alps, about 5 km west of Sierre (Figure 1a). The valley runs from east–northeast to west–southwest. The profile starts at 2,543 m a.s.l. close to the summit of Bella Lui, stretches down the southern exposed (S) slope, through Crans–Montana down to the alluvial valley plain at about 500 m a.s.l., and then ascends the northern exposed (N) slope up to its southernmost point at 2,543 m a.s.l. close to Mont Noble (Figures 1b and 2). The elevational range between the valley base and the upper ends of the transect is about 2,000 m on both slopes.

Tectonically, the S slope belongs to the Helvetic facies with alternating layers of limestone and schist, whereas the N slope belongs to the Penninic facies consisting of Triassic limestone, dolomite, quartzite, and hard crystalline rocks (Gutersohn 1961).

The valley was strongly influenced by glacial processes during the Pleistocene and superimposed by gravitational processes in the Holocene. The tectonic–geological setting combined with geomorphic processes has engendered a considerably asymmetric cross-profile of the valley along the studied transect (Figure 2): due to its harder rocks (Gutersohn 1961), the N slope with a mean inclination of 21.5° is nearly 10° steeper than the S slope (11.8°). Even if the distinct Crans–Montana terrace is excluded, the S slope's mean inclination only reaches 13.2°. The structuring of the S slope in terraces and steeper sections in between can be attributed to the alternating softer and harder rock layers described above, whereas such a distinct layering is missing on the N slope, resulting in a more homogenous relief.

The climate of the study area is relatively dry. The mean yearly precipitation in the valley bottom was 500 to 700 mm in the reference period 1981 to 2010 (MeteoSwiss 2020a). Elevational precipitation gradients on the S slope for the same period are about 10 mm/100 m ascent between 500 and 1,500 m a.s.l. but about ten times higher between 1,500 and 3,200 m a.s.l.

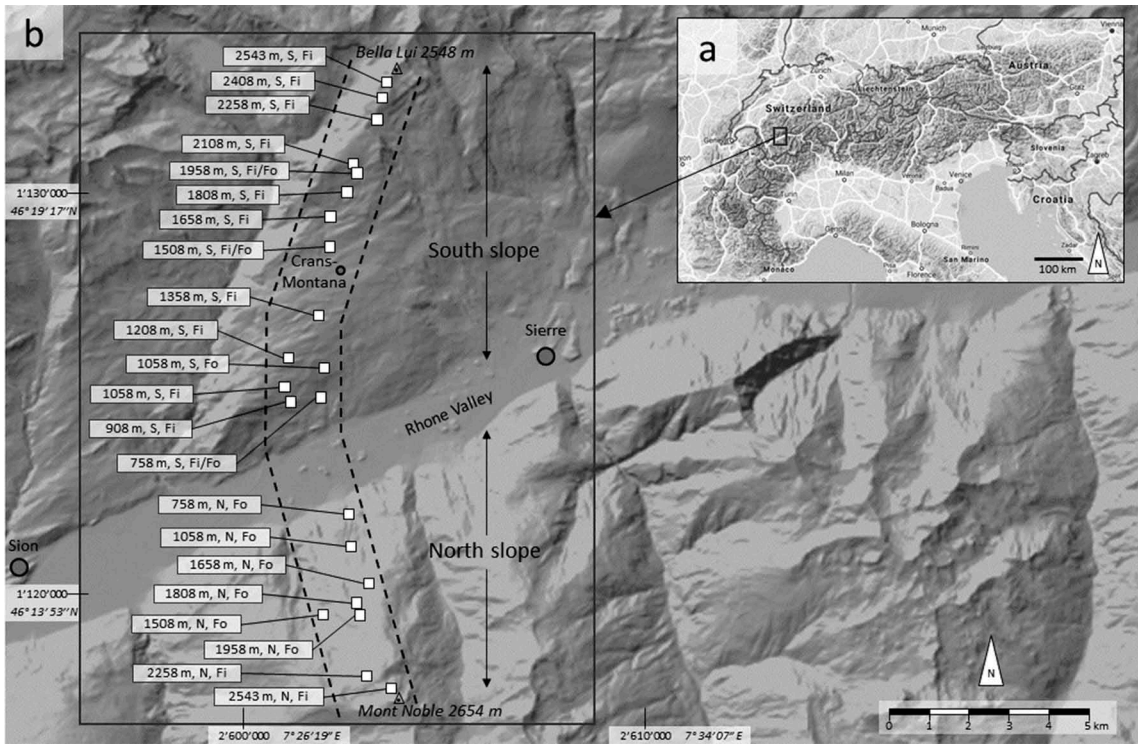

Figure 1. Plan view of the study area and study site. (a) Overview map of the European Alps with the small rectangle indicating the location of the study area. (b) Section of the topographic map covering the study area (large rectangular frame) within which the transect along the measuring plots (squares)—that is, the study site—is delineated by the two dashed lines. The flags pointing to the squares indicate elevation, slope aspect (north or south), land cover (open field or forest). Note the separate plots for field and forest at 1,058 m a.s.l. on the S slope, because the measurements in the field and forest were not adjacent here. The coordinates of the grid lines in map (b) are given in the Swiss coordinate system (normal font) and the World Geodetic System (WGS84; italics). Source of background maps: (a) Google Maps (© Google, n.d.) and (b) Swiss Federal Office of Topography (© swisstopo, 2018). Fi = open field; Fo = forest.

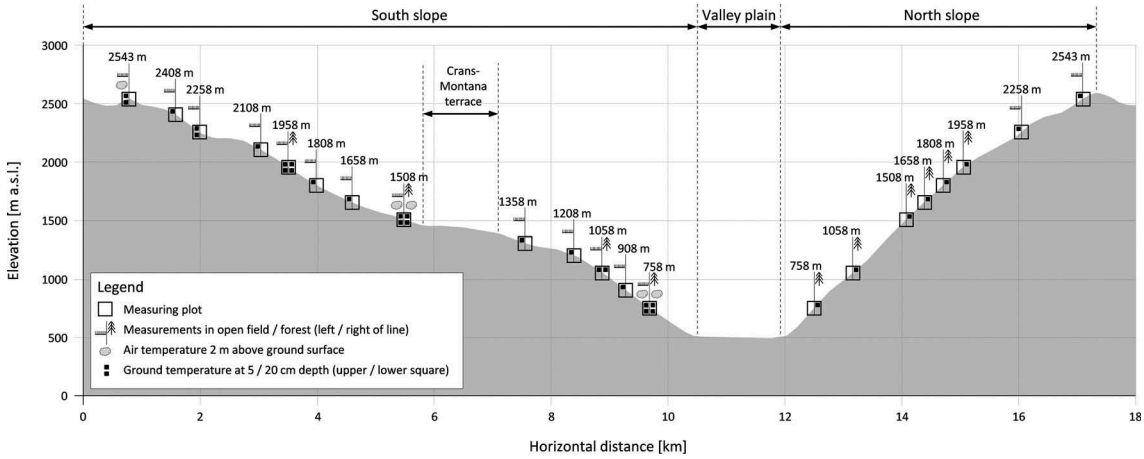

Figure 2. Elevational cross-profile through the Rhone valley near Sierre (Figure 1b) along the measurement transect. South slope = southern exposed (S) slope; North slope = northern exposed (N) slope.

(MeteoSwiss 2017b). Mean annual air temperature ranges between about 8°C and 10°C in the valley, whereby the lowermost 100–200 m of the S slope exceed these temperatures and includes the hottest areas. With absolute sunshine durations of over 2,000 hours per year (e.g., Crans-Montana, MeteoSwiss 2016a; Sion, MeteoSwiss 2016b) and mean yearly relative sunshine durations (measured to maximum possible sunshine duration) of

54 percent up to 60 percent, the Rhone valley is one of the sunniest regions in Switzerland (MeteoSwiss 2020b). In Sion, the ground was snow covered for 8.3 days per year on average (MeteoSwiss 2016b), and in Crans–Montana, which is about 1,000 m higher, for 44.2 days (MeteoSwiss 2016a; reference period 1981–2010). Regarding seasonality of dryness, the study area can be characterized as being summer-dry. This implies that the proportion of snow to rain is higher in the western Swiss inner Alpine valleys than in the eastern ones (such as the Engadin valley in Grisons) with otherwise similar conditions. Due to the dry climate, coniferous trees dominate this type of landscape more strongly than broadleaved or mixed forests (Camenzind et al. 2011). The agricultural land is used for pastures and fodder farming.

On the N slope, forest dominates up to the timberline at around 2,150 m a.s.l. On the S slope, the portions of field and forest are roughly balanced below the timberline, which is at a similar elevation. These differences in land cover between the N and S slopes can be attributed to the slope aspect and inclination. On the flatter, sunny S slope, the cultivation of grassland is possible, whereas the steep and shady N slope is more suitable for forest.

Experimental setup and instrumentation

Along the transect, air and near-surface ground temperatures (T_a and T_g, respectively) were measured between elevations of 758 and 2,543 m a.s.l. (Figures 1 and 2). On the S slope, T_g was measured at thirteen different elevations, and on the N slope T_g was measured at eight elevations. On the S slope, T_g was measured in open fields at all thirteen plots as well as in forests at four plots that were more or less evenly distributed between the valley plain and the timberline. These forest measurements were conducted directly adjacent to the equivalent measurements at the same elevation in the open field, referred to as "field" in the following. However, this arrangement was not possible on the S slope at 1,058 m a.s.l. The measuring points for field and forest at this elevation were at a distance of about 1 km. On the N slope, only forested plots were available below the timberline. T_a was measured at three plots more or less evenly distributed over the S slope. These measurements were performed in the field and forest at the lower two plots at 758 and 1,508 m a.s.l. and in the field only for the uppermost plot at 2,543 m a.s.l. because it is above the timberline.

At all measuring points on the S and N slopes, T_g was recorded at a 5 cm depth below the ground surface. On the S slope, additional measurements at 20 cm depth were conducted at 758, 1,508, and 1,958 m a.s.l. for field and forest and additionally at 2,258 and 2,543 m a.s.l. in the field. T_a was recorded 2 m above the ground surface. All measurements were taken from 4 October 2001 to 3 October 2002 at intervals of 2 hours. The temperatures were measured and recorded by universal temperature loggers (UTLs) from Geotest Ltd. (Switzerland). The UTL has a resolution of 0.27°C and a measuring accuracy of 0.1°C within the measurement range from −29°C to +39°C. All UTLs were calibrated before field use in a continuously stirred ice water mixture at 0°C. The UTLs were buried into the ground with the sensor at the respective depth. The natural ground structure was disturbed minimally. During placement, thermal contact between the sensor and the surrounding ground was established. T_a was measured with the UTL on a pole and shielded from radiation.

Additional data

In order to calculate mean daily, winter, summer, and annual air temperatures along the N slope of the study area T_a data from the weather stations at Sion (482 m a.s.l., coordinates 2'591'630 E / 1'118'575 N) in the Rhone valley plain and at Les Attelas (2,730 m a.s.l., coordinates 2'586'862 E / 1'105'305 N) on the N slope slightly higher than Mont Noble (2,543 m a.s.l.) and 21 km southwest were used (MeteoSwiss 2017a). Both stations are in fields. These additional data covered the same period as the data presented in this study. The additional T_a data had a temporal resolution of one day.

Determination of missing air temperatures

The missing T_a values on the N slope (Figure 2) were determined using elevational T_a gradients between the weather stations at Sion and Les Attelas managed by MeteoSwiss (2017a). T_a was linearly interpolated between these two weather stations for the plots on the N slope (Figures 1 and 2). According to a linear T_a gradient derived from T_a measurements on the opposite slope, linearity could also be adopted for the N slope. Because the weather stations are in fields, the derived T_a for the N slope also refer to the field. On the S slope, T_a was linearly interpolated between the plots measuring T_a (Figure 2) for plots measuring only T_g.

Data processing and derivation of further thermal parameters

First, the deviation of each T_g series from 0°C at the zero curtain (i.e., the period of phase change during which water and ice coexist and thus T_g has to remain constant at 0°C for thermodynamic reasons) was determined. These deviations were then subtracted from the respective T_g series of raw data to achieve correct T_g values. Then daily mean,

maximum, and minimum T_a and T_g were calculated from 2-hourly data. T_a maxima and minima were used to determine for each day whether it was an ice day (i.e., T_a maximum <0°C), a frost day (i.e., T_a minimum <0°C), a frost change day (i.e., a frost day that was not an ice day), or a frost-free day. These technical terms originally used for the atmospheric air were transferred to the ground, resulting in the equivalent ground parameters. The T_g change with depth—that is, the temperature/depth gradient (T_g/z)—was calculated by daily mean, maximum, and minimum T_g data at 5 and 20 cm depths where T_g was measured at both depths at 758, 1,508, 2,258, and 2,543 m a.s.l. on the S slope in the field (Figure 2).

The snow cover period for each plot was determined by means of T_g at 5 cm depth with a 2-hourly resolution. A necessary condition for a day with snow cover is that subdaily T_g variations suspend. However, if this condition is fulfilled for a day but before T_g decreases to 0°C, then roughly stays constant, and thereafter varies subdaily either above or below 0°C, there is not necessarily snow cover on this day. Measurements of near-surface ground temperatures and snow depth at the same site in the Swiss Alps by Matsuoka et al. (1997) and Matsuoka (2001) showed that the snow cover period can be inferred from near-surface ground temperatures. This method was thus applied in this study as well.

For the daily means, maxima, and minima of T_a, T_g, and T_g/z, the means over the three coldest months (December, January, and February; referred to as winter) and hottest months (June, July, and August; referred to as summer) were determined. The number of ice and frost change days (ID and FCD, respectively) for air and ground were summarized over a year, resulting in ID_a and FCD_a for air and ID_g and FCD_g for ground. Note that the yearly sum of frost days is just the yearly sum of ice and frost change days and is thus not considered here. In addition, the first freezing ($FD1_g$) and thawing day ($TD1_g$) were determined; that is, the first days of the year for which the mean daily T_g was below 0°C and above 0°C, respectively. Furthermore, the first snow-free day of the year (SFD1) was determined as indicated by a sudden beginning of pronounced T_g variations at 5 cm depth after a long period of marginal variations due to thermal insulation and shielding by the snow cover. $TD1_g$ and SFD1 occurred in the same calendar year at all measuring points but $FD1_g$ occurred in 2002 at some measuring points, in 2001 at others. To compare all measuring points with regard to $FD1_g$, 365 days (of the year 2001) were subtracted if $FD1_g$ occurred in 2001. The days of the year with snow cover were summed to the snow cover days (SCDs) for each plot. The parameters analyzed in the study are provided in Table 1. Ground parameters refer to 5 cm depth, and the T_g/z gradient refers to a depth range from 5 to 20 cm.

Data analysis

The data were analyzed using the statistical software R and Microsoft Excel. For the subdaily data and the daily aggregated data (Table 1), time series analyses were performed. Air vs. ground parameters, low vs. high elevations, and mean vs. night vs. daytime values were compared.

Table 1. Thermal air and ground parameters analyzed in this study.

					Granularity				
Medium	Parameter	Symbol	Unit	2 Hours	Day	Winter	Summer	Year
Air	Air temperature	T_a	°C	x				
	Daily mean				x	x	x	x
	Daily maximum (day)					x	x	
	Daily minimum (night)					x	x	
	Ice days in the air	ID_a	Day					x
	Frost change days in the air	FCD_a	Day					x
Ground	Ground temperature	T_g	°C	x				
	Daily mean				x	x	x	x
	Daily maximum (day)					x	x	x
	Daily minimum (night)					x	x	x
	Ice days in the ground	ID_g	Day					x
	Frost change days in the ground	FCD_g	Day					x
	First freezing day of the year in the ground	$FD1_g$	Day					x
	First thawing day of the year in the ground	$TD1_g$	Day					x
	Ground temperature/depth gradient	T_g/z	°C/m					
	Daily mean					x	x	x
	Daily maximum (day)					x	x	x
	Daily minimum (night)					x	x	x
Snow	Snow cover period/days	SCD	Day		x			x
	First snow-free day of the year	SFD1	Day					x

Note. For further details see text of subsection "Data processing and derivation of further thermal parameters."

For the analysis of the yearly aggregated data (Table 1), three different data sets were compiled to analyze (1) the effect of elevation on ground and air thermal parameters in general, (2) these elevational thermal gradients with respect to slope aspect (N slope vs. S slope) and (3) these elevational thermal gradients with respect to land cover (field vs. forest). Data set 1 includes data from all thirteen plots on the S slope in the field (for air and ground parameters; Figure 2). For data set 2, data from four plots at 758, 1,058, 1,508, and 1,958 m a.s.l. on the S and N slopes were compiled. Because the N slope is completely forested up to the timberline, ground parameters refer to forest. However, no air temperatures under forest were available on the N slope. They were thus derived by means of nearby meteorological stations (see "Additional data" and "Determination of missing air temperatures" sections) situated in the field. Because air temperatures refer to field on the N slope, field air temperatures were also used on the S slope. For data set 3, data were used from plots on the S slope in the field and forest at the same elevations used for data set 2 and additionally from field plots at 908, 1,208, 1,358, and 1,808 m a.s.l. Taking data from four elevations in the forest and eight in the field for data set 3 allowed better utilization of the available data. Because the mean elevation for both forest and field is 1,321 m a.s.l. in data set 3, the data were balanced and effects were not confounded.

For all parameters within each data set, regressions on the main factor elevation were calculated. In data set 1, a linear regression model was established for each parameter. In order to determine whether the coefficient of determination, R^2, increased, linear models with Box-Cox-transformed data as well as second- or third-order polynomial models were applied thereafter, but overfitting was avoided. The Box-Cox transformation of a target variable Y (e.g., the number of ice days) is based on Equation (1):

$$box.cox(Y,\lambda) = \frac{Y^{\lambda} - 1}{\lambda} \quad (1)$$

where λ is the optimal power parameter to obtain a linear relation between the factor elevation and Y. Whether the assumptions were fulfilled was determined for all regressions; that is, normal distribution, homogeneity of variance, no outliers, and no autocorrelation. Regression lines were also fitted to interpolated data and exponential functions were tested in case the data suggested this kind of relation. However, no R^2 could be assigned to these regressions.

Equivalent statistical analyses were applied to the other two data sets. However, for each parameter, regression lines between north and south (data set 2) and field and forest (data set 3) were compared. If a nonlinear regression line was determined for a parameter by thirteen data points from data set 1 (e.g., a sigmoid curve), this type of curve was predefined for regressions of the same parameter in data set 2 or 3 with fewer data points.

Results

The results are divided into three subsections. The first subsection presents the elevational thermal gradients in general; that is, it focuses on how thermal parameters depend on elevation as a main factor. The following subsections present the elevational thermal gradients separated by the co-factors slope aspect and land cover.

Elevational thermal gradients—Generally

Unless specified differently, the results presented in this subsection refer to the S slope and field because for this factor combination data are available at all investigated elevations, which is the main focus here.

Subdaily data

Air and ground temperatures show a distinct subdaily course over the whole elevational range in summer (Figure 3). Ground temperatures (T_g) follow the air temperature (T_a) courses typically with a time lag of about 2 hours. Sometimes they apparently coincide due to the measuring resolution of 2 hours (Figure 3; 3 July 2001, 758 m a.s.l.). At different elevations the respective temperature maxima and minima might occur simultaneously (Figure 3; 1 July 2001) or slightly shifted (2 July 2001).

Within the period shown in Figure 3, T_a ranges between about 12°C and 27°C at 758 m a.s.l. and T_g ranges between about 18°C and 23°C. At this elevation, the subdaily amplitude of T_a is about 10°C to 15°C but is only 3°C to 5°C for T_g. In contrast, at 2,543 m a.s.l., T_g ranges between about 6°C and 16°C and is always higher than T_a, which ranges between about 3°C and 11°C. At this elevation, the subdaily amplitude of T_a is about 5°C to 8°C and that of T_g is 5°C to 10°C.

Daily aggregated data

Air and ground temperatures show an oscillating yearly course, with high values in summer and low ones in winter, and the overall temperature levels decrease with elevation (Figure 4). However, whereas air temperatures (T_a) strongly vary throughout the year, ground temperatures (T_g) remain constant at about 0°C in winter for a period of time and are decoupled from

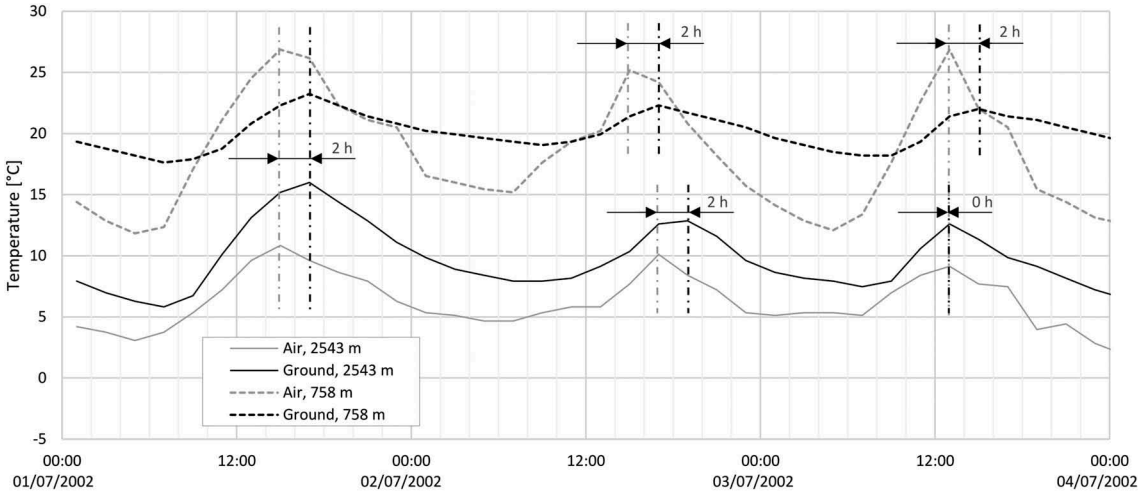

Figure 3. Typical subdaily air and ground temperature courses in summer at the lowermost and uppermost ends of the elevational transect on the S slope in the field. Note that the measurement resolution was 2 hours. Dates (d/m/y).

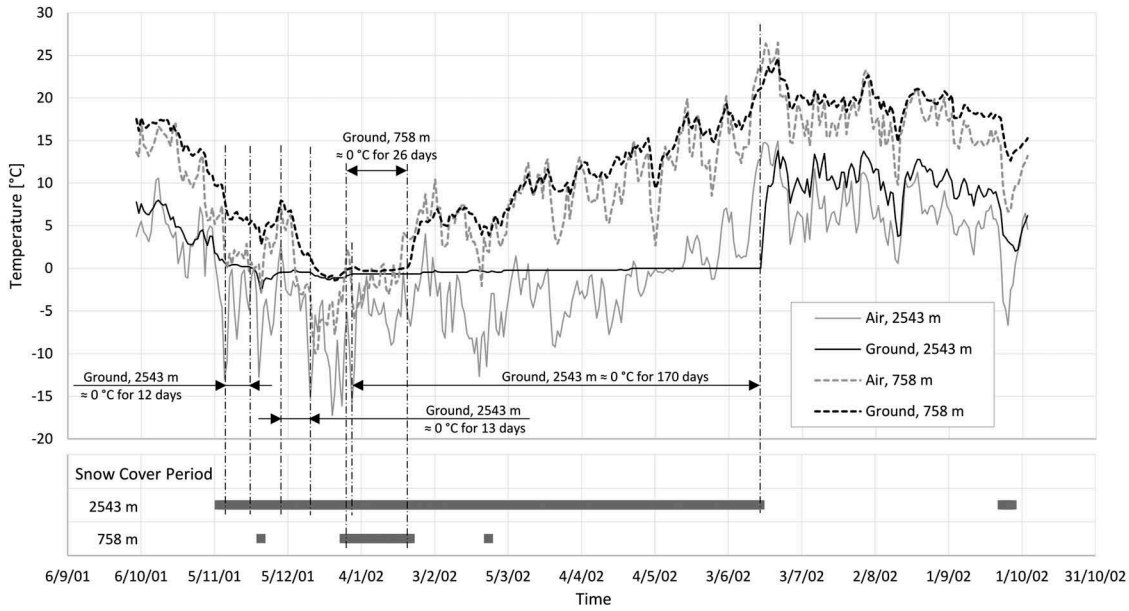

Figure 4. Air and ground temperature courses on the basis of daily mean values and snow cover period at the lowermost and uppermost ends of the elevational transect on the S slope in the field. Dates (d/m/y).

T_a variations. This 0°C period lasts less than a month at 758 m a.s.l. but over half a year at 2,543 m a.s.l. (Figure 4). For both elevations this period occurs under snow, whereas the end of the 0°C period and the snow cover period roughly coincide. Moreover, outside this period T_g varies much less than T_a, especially below the freezing point. Above the freezing point, T_g exceeds T_a more often than T_a exceeds T_g. This effect is stronger at high elevations (2,543 m a.s.l.) than close to the valley (758 m a.s.l.).

The length of the snow cover period increases from the valley upslope (Figure 5). Whereas this period is roughly continuous at higher elevations, it becomes increasingly fragmented downslope. The onset of the snow cover in autumn occurs simultaneously over wide elevational ranges; for example, on 7 November 2001 above 1,900 m a.s.l. The onset at 758 m a.s.l. is delayed to that at 2,543 m a.s.l. by only twenty-seven days. In contrast, the termination of the snow cover in spring spreads much longer over the elevational gradient, namely, from 25 February 2002 at 758 m a.s.l. until 16 June 2002 at 2,543 m a.s.l., nearly four months. Moreover, for the S slope field, snow cover termination is delayed with increasing elevation only slightly up to

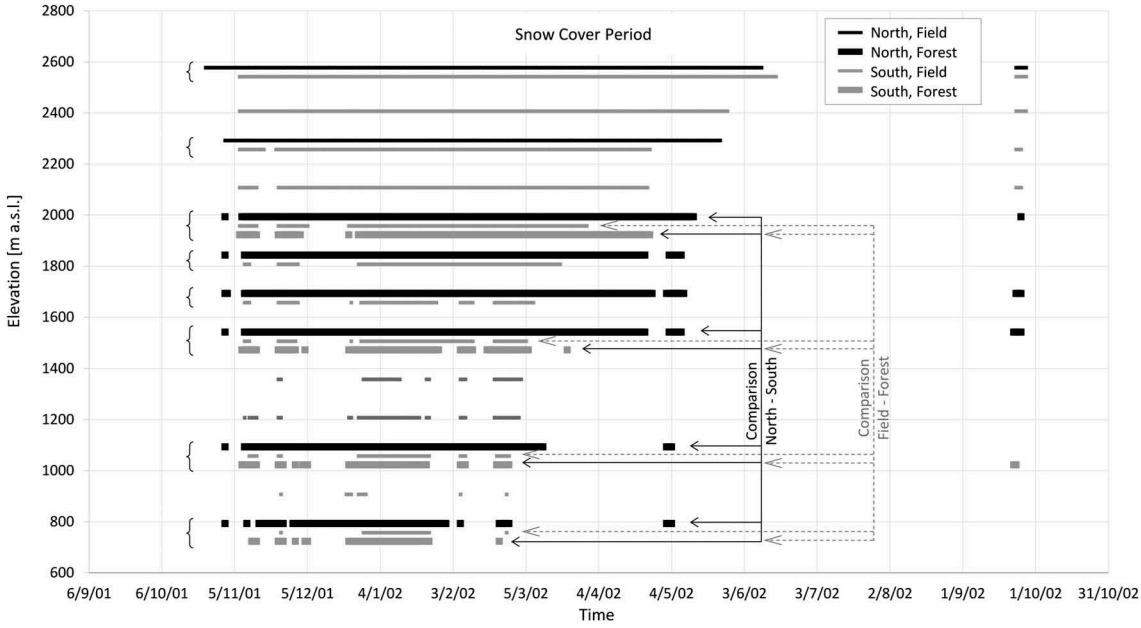

Figure 5. Periods of snow cover for the measuring plots along the elevational gradient. In order to distinguish the bars of different aspects and land covers at the same elevation those for "north, field," "north, forest," and "south, forest" are displayed slightly shifted vertically and those for "south, field" are displayed at the real elevation. Braces indicate bars at the same elevation. Dates (d/m/y).

about 1,600 m a.s.l. but progressively more above this elevation. A short snow cover phase in early autumn took place only above 2,000 m a.s.l.

Yearly aggregated data

During the observation period, the yearly mean air temperature (T_a) was 10°C on the S slope close to the valley bottom and decreased by 0.53°C/100 m elevation (Figure 6a). The regression line for the yearly mean of the ground temperatures (T_g) runs roughly parallel but 3°C higher. Below 1,250 m a.s.l., the difference between T_a and T_g becomes smaller to reach less than 2°C at 700 m a.s.l. The yearly mean T_g gradient over the observed elevational range is 0.44°C/100 m. In contrast to the mean elevational T_a gradients based on mean daily values being linear in winter (Figure 6c) and summer (Figure 6d), the equivalent gradients for the ground are curved (Figures 6g, 6h).

The day–night amplitude of the yearly mean of T_g decreases from 4.0°C at 700 m a.s.l. to 2.7°C at 2,500 m a.s.l. (Figure 6b). Whereas T_g data points for the night are situated close to the regression line, the daytime values are much more scattered below about 1,800 m a.s.l. In winter, the day–night amplitude of T_g drops to 1.9°C at 700 m a.s.l. and continuously decreases with elevation to completely disappear at 2,500 m a.s.l. (Figure 6g). However, because the elevational T_g gradient is quite flat in winter (roughly −0.2°C/100 m) the subdaily variation in the 0°C line (i.e., the elevation at which 0°C prevails) is ±100 m around the daily winter mean of about 2,000 m a.s.l. In contrast to T_g, T_a in winter shows subdaily variation of 6.7°C at 700 m a.s.l., 8.0°C at 1,650 m a.s.l., and 5.2°C at 2,600 m a.s.l. (Figure 6c), so for a medium elevation twelve times more than T_g. In summer, the subdaily T_a amplitude is about 12°C at 700 m a.s.l. and reduces to 8.5°C at 2,600 m a.s.l. (Figure 6d). It is thus still three times higher than that for T_g at 700 m a.s.l. but nearly equal at 2,600 m a.s.l. (Figure 6h).

The seasonal temperature amplitudes in the air and the ground are defined here as the difference between mean summer and winter temperatures. According to Figures 6c and 6d, the seasonal T_a amplitude is 17.3°C at 700 m a.s.l., 14.8°C at 1,650 m a.s.l., and 13.0°C at 2,600 m a.s.l. For T_g it is only 0.4°C lower at 700 and 1,650 m a.s.l. but 4.5°C lower at 2,600 m a.s.l. (Figures 6g, 6h).

The number of ice days is about the same (fifteen) for air and ground at 700 m a.s.l. according to the regression lines (Figure 6e). Both increase progressively with elevation but more so for the ground, resulting in nearly 150 air ice days and 200 ground ice days at 2,600 m a.s.l. However, the data points for the ground scatter considerably around the regression line. The number of frost change days in the air first increases with elevation, reaches a local maximum of 146 days at about 1,900 m a.s.l., and decreases above 1,900 m a.s.l. (Figure 6f). The number of ground frost change days is marginal compared to air and reaches mostly one-digit values at 2,258 m a.s.l. (sixteen days) and

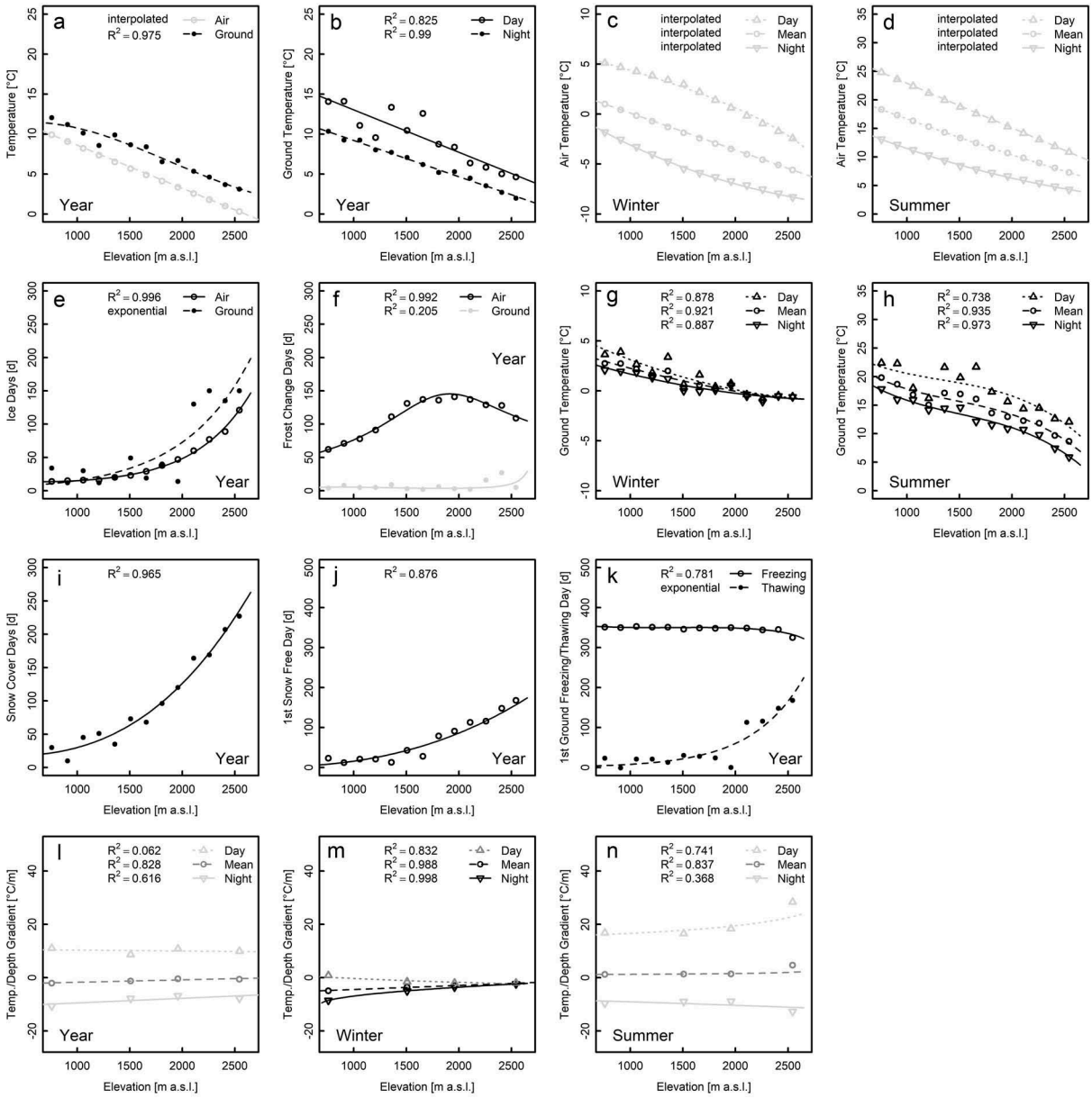

Figure 6. Diagrams for regressions of air and ground thermal parameters on elevation. All data refer to the S slope and the open field. Winter refers to data from December to February; summer refers to data from June to August. Note that if regressions are based on interpolated data or if an exponential regression line was fitted to the data, no coefficient of determination, R^2, could be calculated. Gray shading for data points and regression lines for significance levels: black for $p \leq .05$, dark gray for $.05 < p \leq .1$, light gray for $p > .1$, where the smallest p value of the coefficients in the regression equation is decisive. Data containing interpolated points and their regression lines are drawn in light gray.

2,408 m a.s.l. (twenty-seven days), leading to a small increasing trend at elevations above 2,200 m a.s.l.

At 700 m a.s.l., the snow cover lasts for about twenty days according to the regression (Figure 6i). The number of snow cover days progressively increases with elevation and reaches about 250 at 2,600 m a.s.l. The first snow-free day after winter occurs at 700 m a.s.l. in the second half of January and becomes increasingly delayed with elevation to occur in the second half of June at 2,600 m a.s.l. (Figure 6j). Thawing at 5 cm depth typically took place on the first snow-free day (Figure 6k). However, at some measuring points (e.g., at 1,808 and 1,958 m a.s.l.), the ground temperature rose slightly above 0°C under the snow cover. The first day of ground freezing appears to be nearly independent of elevation (Figure 6k). However, whereas it occurs in mid-December at 700 m a.s.l.,

it becomes gradually earlier with elevation and slightly steepens above 2,300 m a.s.l. to occur in the middle to the end of November at 2,600 m a.s.l.

The mean daily temperature/depth gradients (T_g/z) appear to be nearly independent of elevation, but they slightly increase with elevation (Figures 6l–6n). Averaged over the year, T_g/z is about 0°C/m (Figure 6l), over winter slightly negative (Figure 6m), and over summer slightly positive (Figure 6n) along the whole elevational gradient. However, whereas T_g/z is negative throughout the day in winter (Figure 6m), it alternates between negative values during the night and positive values during the day (Figure 6n). Moreover, its subdaily amplitude in winter is about 9°C/m and diminishes with elevation to disappear at about 2,500 m a.s.l. In contrast, the subdaily amplitude of the temperature/depth gradient in summer increases from about 25°C/m at 700m a.s.l. to about 40°C/m at 2,600 m a.s.l. in a trumpet-like pattern.

Elevational thermal gradients—Separated by slope aspect

The mean annual air temperature (T_a) on the N slope (9.4°C) is only 0.8°C lower than that on the S slope at 700 m a.s.l. (Figure 7a). This difference diminishes with elevation and disappears above about 2,000 m a.s.l. The elevational T_a gradient is thus slightly steeper for the S slope (−0.54°C/100 m) than for the N slope (−0.48°C/100 m). The influence of the slope aspect is more pronounced for ground temperatures (T_g; Figure 7b): at 700 m a.s.l. the difference between the N and S slopes is 1.9°C and the elevational T_g gradients differ more than for T_a regarding aspect with values of −0.38°C/100 m for the N slope and −0.5°C/100 m for the S slope. The T_g regression lines for N and S slopes intersect at about 2,200 m a.s.l.

In summer, T_g are equal for the N and S slopes at 700 m a.s.l. (Figures 7d, 7h) and slightly diverge with

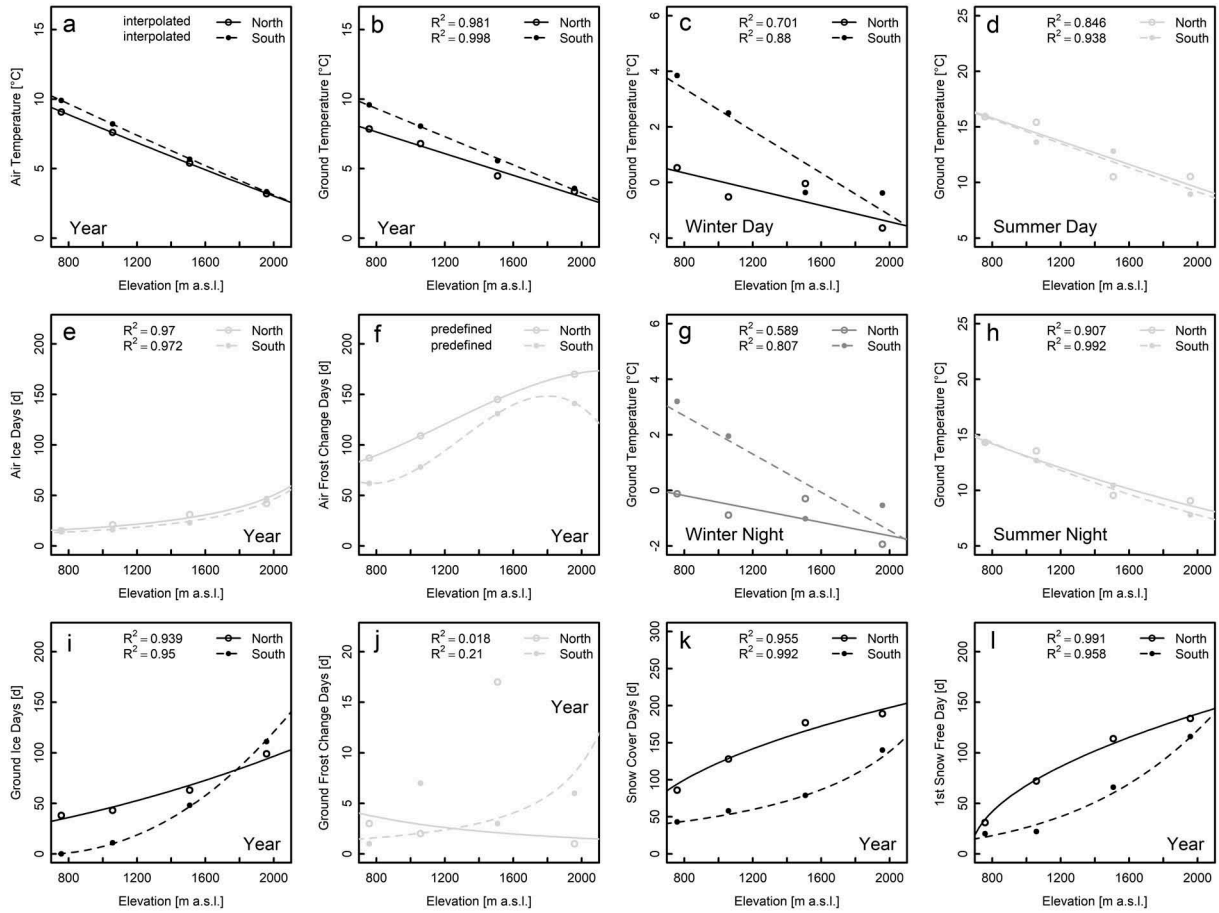

Figure 7. Diagrams for regressions of air and ground thermal parameters on elevation with respect to slope aspect. Air data refer to the open field and ground data to forest and 5 cm depth below surface. Gray shading for data points and regression lines for significance levels regarding the difference between north and south: black for $p \leq .05$, dark gray for $.05 < p \leq .1$, light gray for $p > .1$, where the smallest p value of the regression coefficients is decisive.

elevation, which is statistically not significant. The subdaily T_g amplitude is equal for N and S slopes at 700 m a.s.l. in summer (1.5°C) and slightly decreases with elevation to 0.9°C on the N slope and 1.3°C on the S slope at 2,100 m a.s.l. The elevational T_g gradients in summer are −0.51°C/100 m for the N slope and −0.54°C/100 m for the S slope.

In contrast to summer, the winterly N–S difference in T_g is highest at 700 m a.s.l. (3.3°C for day and night) and decreases with elevation (Figures 7c, 7g) to cease at 2,100 m a.s.l. where T_g is −1.6°C during the day and −1.8°C at night. The subdaily T_g amplitude in winter is identical for N and S slopes and marginal (0.6°C at 700 m a.s.l. and 0.2°C at 2,100 m a.s.l.). In winter, the elevational T_g gradient on the S slope (−0.36°C/100 m) is nearly three times higher than that on the N slope (−0.13°C/100 m). Therefore, the 0°C line during a winter day lies at about 1,700 m a.s.l. on the S slope and more than 600 m lower on the N slope. This difference increases to 900 m at night.

The regression lines for the number of ice days in the air (ID_a) with respect to slope aspect run roughly parallel, differing by two to four days (Figure 7e). The progressive increase in ID_a with elevation observed in Figure 7e is also valid for the N slope. In contrast to ID_a, the number of ground ice days (ID_g) differs more strongly between N and S slopes (Figure 7i): Whereas there were thirty-two ID_g at 700 m a.s.l. on the N slope, but none on the S slope, ID_g for the S slope increases more with elevation than for the N slope. The N and S curves for ID_g intersect at 1,800 m a.s.l. and eighty-two days. Upslope ID_g rises faster on the S slope than on the N slope.

The curve for frost change days in the air (FCD_a; Figure 7f) on the S slope has a local maximum between 1,800 and 1,900 m a.s.l. with nearly 150 FCD_a and roughly equals the one shown in Figure 6f. This sigmoid shape applies for the N slope as well, but a local maximum does not occur in the observed elevational range. The FCD_a curve for the N slope increases with elevation, slightly flattening. Averaged over elevation, twenty-five more FCD_a occur on the N slope than on the S slope. In contrast, ground frost change days (FCD_g) are marginal, not only on the S slope (shown in Figure 6f) but also on the N slope (Figure 7j). A significant correlation with elevation is lacking. Note the factor of ten between the ordinates of the FCD_g and FCD_a plot.

Whereas the curves for snow cover days (SCDs) and the first snow-free day of the year (SFD1) increase progressively with elevation (Figures 6i, 6j) on the S slope, they run at a higher level on the N slope but increase degressively upslope (Figures 7k, 7l). Consequently, the N–S differences regarding SCD and SFD1 increase upslope to about 1,400 m a.s.l. and decrease thereafter.

Elevational thermal gradients—Separated by land cover

On the plots for the field–forest comparison, the snow cover periods are longer for forest than for field at the same elevation but are more fragmented (Figure 5). The onset of snow cover occurs earlier for forest than field—twelve days at 758 m a.s.l.—but progressively less upslope. In contrast, the snow cover terminates three days later for field than forest at 758 m a.s.l., on the same day at 1,058 m a.s.l., but seventeen days earlier at 1,508 m a.s.l., and twenty-six days earlier at 1,958 m a.s.l.

In the forest, the yearly mean air temperature (T_a) depending on elevation is only marginally lower (<0.2°C on average), and its elevational gradient slightly is steeper (−0.55°C/100 m) than in the field (−0.54°C/100 m; Figure 8a). The yearly mean ground temperature (T_g) is quite similar to T_a for forest, whereas it is 2.1°C (700 m a.s.l.) to 3.0°C (2,100 m a.s.l.) higher in the field (Figure 8b). Accordingly, the elevational T_g gradient is similar to that of T_a for forest (−0.51°C/100 m) but clearly flatter for field (−0.45°C/100 m).

For summer nights, the T_g differences with respect to land cover are around 3°C and thus are similar to those of the yearly mean (Figure 8h). However, during daytime, the differences considerably increase to 5.0°C at 700 m a.s.l. and 6.9°C at 2,100 m a.s.l. (Figure 8d). Therefore, the T_g gradient under forest is 0.13°C/100 m steeper than in the field. The subdaily T_g amplitude in summer is about 1.8°C under forest and nearly constant with elevation but two (700 m a.s.l.) to three (2,100 m a.s.l.) times higher in the field.

Whereas T_g in summer is higher in the field than in the forest during the day and at night over the entire elevational range, this is true in winter only during the day (Figures 8c, 8g). At this time, T_g is only marginally higher in the field at 700 m a.s.l., but this difference increases upslope to about 1°C at 1,600 m a.s.l. and remains constant above (Figure 8c). During a typical winter day, the 0°C line differs by more than 600 m between forest (1,600 m a.s.l.) and field (over 2,200 m a.s.l.). During winter nights the ground is warmer in the forest than in the field up to about 1,300 m a.s.l. and cooler above this elevation. The overall elevational T_g gradient is −0.17°C/100 m in the field and more than twice as high under forest. Whereas the 0°C line during the night remains at about the same elevation as during day under forest, it is about 300 m deeper at night compared to day-

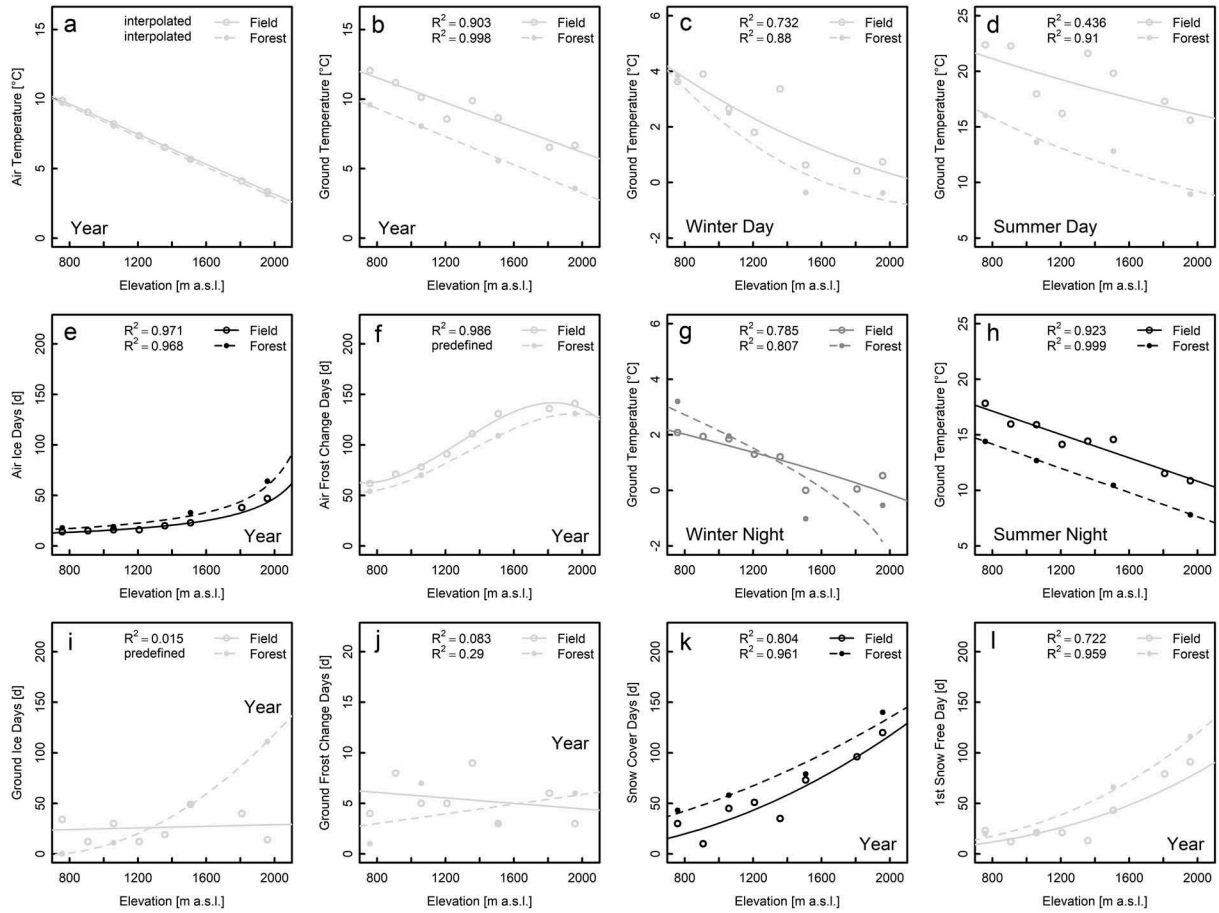

Figure 8. Diagrams for regressions of air and ground thermal parameters on elevation with respect to the land cover. All data refer to the S slope and ground data refer to 5 cm depth. Gray shading for data points and regression lines for significance levels regarding the difference between field and forest: black for $p \leq .05$, dark gray for $.05 < p \leq .1$, light gray for $p > .1$, where the smallest p value of the regression coefficients is decisive. Filled large circles in (a), (i), (j), and (l) indicate that data points for field and forest are superimposed.

time in the field. The subdaily T_g amplitude in winter is higher in the field (2.0°C) than in the forest (1.0°C) at 700 m a.s.l. but higher in the forest (2.1°C) than in the field (0.2°C) at 2,100 m a.s.l. The seasonal T_g difference between winter and summer is 16.7°C at 700 m a.s.l. and 12.8°C at 2,100 m a.s.l. in the field and thus 3.1°C (2,100 m a.s.l.) to 4.4°C (700 m a.s.l.) higher than in the forest.

Ice days of the air (ID_a) are more frequent under forest than in the field (Figure 8e). The difference is marginal at 700 m a.s.l. but progressively increases with elevation to about thirty ID_a at 2,100 m a.s.l.; that is, one third of ID_a in the forest. Ground ice days (ID_g) behave completely different for field and forest (Figure 8i). In the field, ID_g values scatter around an average of twenty-six days without an upslope trend. In the forest, no ID_g appear at 700 m a.s.l., but the regression line progressively increases with elevation, intersects the one for field at about 1,300 m a.s.l., and reaches 137 ID_g at 2,100 m a.s.l.

Air frost change days (FCD_a) occur more frequently in the field than under forest (Figure 8f), and both regression lines follow a sigmoid course (Figure 8f). In the field the maximum takes place at 1,830 m a.s.l., reaching 142 FCD_a, and the maximum takes place in the forest at 1,990 m a.s.l. and 131 FCD_a.

The finding that the number of frost change days in the ground (FCD_g) is marginal compared to FCD_a and is not correlated to elevation (Figure 7f) proves true for forest also (Figure 8j). FCD_g is about five averaged over the whole slope for both types of land cover. The different trends with elevation are statistically not significant.

In the forest, the ground is covered by snow for a longer period, namely 38 days compared to 16 days in the field at 700 m a.s.l. and 144 days compared to

128 days in the field at 2,100 m a.s.l. (Figure 8k). That means that the difference between field and forest regarding snow cover days (SCDs) reduces with elevation. In contrast, the difference between field and forest concerning the first snow-free day after winter progressively increases with elevation: At 700 m a.s.l., the forest lags 4 days behind the field, and at 2,100 m a.s.l. it lags by 45 days; that is, more than a tenfold increase.

Discussion

Elevational thermal gradients—Generally

Subdaily and daily aggregated data

On a subdaily scale of temperature courses (Figure 3), it can be recognized that the ground temperature (T_g) follows the air temperature (T_a) if the ground is in direct contact with the atmosphere; that is, without snow cover. This suggests the influence of T_a on T_g.

Furthermore, the lower maxima and subdiurnal amplitudes of T_g compared to equivalent values of T_a at 758 m a.s.l. indicate that the T_a signal is damped in the ground. However, this is not the case at 2,543 m a.s.l., where T_g is always above T_a. This difference between the low and high elevation regarding T_a and T_g can plausibly be explained by the ground's grain size distribution, its water content, and radiation, although these parameters were not measured in the study.

At 758 m a.s.l., the ground is much finer grained than at 2,543 m a.s.l., where scree is dominant. Because the water storage capacity is higher for fine-grained subtrates than for coarse-grained substrates (Hillel 2004), the water content of the near-surface ground should be markedly higher at lower elevation than at higher elevation. In turn, both the thermal heat conductivity and volumetric heat capacity of the ground strongly increase with its water content (Hillel 2004). Furthermore, far less solar radiation reaches the ground surface at 758 m a.s.l. than at 2,543 m a.s.l. (Barry 2008). Consequently, during daytime heat originating from the atmospheric air and caused by incoming radiation at the ground surface is rapidly conducted and thus distributed to depth at 758 m a.s.l. Additionally, due to the high heat capacity at this elevation, large amounts of heat are necessary for a given volume to cause a given temperature change. Large amounts of heat can be stored in the ground during daytime. Both ground properties at 758 m a.s.l., the high thermal conductivity and the high heat capacity, result in relatively low daily maximum values of T_g compared to T_a. However, because large amounts of heat energy are stored during the daytime and the outgoing radiation is relatively low at night (compared to higher elevations), ground cooling is moderate and T_g minima are relatively high compared to those of T_a.

In contrast, at 2,543 m a.s.l., the high incoming radiation strongly heats up the ground surface. Due to the low thermal conductivity at this elevation, the heat is concentrated in the uppermost layer where the T_g increase induced thereby is intensified due to the low heat capacity. Both effects lead to high T_g maxima exceeding those of T_a at 2,543 m a.s.l. At night, however, less heat energy can be stored in the ground compared to lower elevations and the outgoing radiation is stronger, resulting in a far higher subdaily T_g amplitude compared to the damped one at 758 m a.s.l.

According to yearly temperature courses based on daily aggregated data (Figure 4), T_a and T_g temporally correlate well outside the snow cover periods and variations are dampened in the ground. However, the marked local T_g minimum at 2,543 m a.s.l. in the second half of November 2001 coincides with a strong local T_a minimum, although snow cover existed at this time (Figure 4). Radiation as a reason for this drop in T_g can be ruled out because it is strongly reflected by snow due to its high albedo. Consequently, the T_g drop below 0°C was caused by the T_a drop. This means that T_a also influences T_g if the snow cover is quite thin, as can be assumed by means of the course of snow depth at the Montana weather station and is very likely for November in the study area. Before and after this period with T_g markedly below 0°C around the T_g minimum, there are periods during which snow is covering and T_g remains constant at roughly 0°C, for twelve and thirteen days, respectively, although T_a strongly varies (Figure 4). A plausible reason for this is the phenomenon of the zero curtain evolving due to the coexistence of water and ice: Under such conditions, T_g must theoretically remain at 0°C for thermodynamic reasons until a phase change (i.e., freezing or thawing) is completed. Only thereafter can T_g decrease below or rise above 0°C. Thus, a zero curtain is also possible without snow cover. However, the abrupt end of the 170-day zero curtain at 2,543 m a.s.l. and only 5 cm below the ground surface coincides quite well with the end of the snow cover period. According to Figure 4, zero curtains of T_g at shallow ground depths and the periods in between below 0°C typically occur under snow cover. On the other hand, periods with a constant T_g at 0°C can also be due to a thermal equilibrium of the near-surface ground, which is stabilized by a well-insulating snow cover. It is thus often not possible to distinguish between a zero curtain and a thermal equilibrium at 0°C unless the T_g sensors are highly accurate.

To estimate snow depth, measurements at the Montana weather station (1,427 m a.s.l.) were considered: Snowfall at the end of November 2001, brought 17 cm of snow. This

snow melted again before the snowfall at the end of December 2001, which brought 45 cm of snow. At 2,543 m a.s.l., these two snowfalls most probably resulted in more than 17 and 45 cm of snow, and the snow from the first event was likely conserved until the next snowfall occurred. This resulted in a snow depth of more than 62 cm at the beginning of the long zero curtain at 2,543 m a.s.l. According to Hanson and Hoelzle (2004), the ground is completely insulated from the atmosphere above a snow depth of about 60 cm. A further indication that the ground at 2,543 m a.s.l. is thermally decoupled from the atmosphere in winter is given in Figure 6m because the T_g/z gradient no longer shows subdaily variation and is roughly zero above 2,500 m a.s.l. in winter. It can thus be concluded that snow cover conserves the zero curtain the longer and deeper it is and the zero curtain ends roughly with snow cover in spring.

Yearly aggregated data

The fact that the mean annual ground temperatures (T_g) are higher than the mean annual air temperatures (T_a) from 700 to 2,600 m a.s.l. (Figure 6a) can be attributed to the direct heating of the ground surface by solar radiation, whereas the air is heated only indirectly and dampened. From the much higher T_g than T_a in winter (Figure 6g) compared to summer (Figure 6h), it can be inferred that in addition to radiation, snow strongly contributes to T_g exceeding T_a with respect to the yearly mean: Snow acts as a thermal insulator and thus protects the ground from the cold atmosphere.

The elevational T_g gradient averaged over the whole elevational range is flatter (i.e., less negative) than that for air (Figure 6a). This finding can be explained by radiation and snow: In summer, the elevational increase in global solar radiation (Barry 2008) flattens the elevational T_g gradient (−0.56°C/100 m; Figure 6h) compared to air (−0.64°C/100 m; Figure 6d); in winter, the elevational increase in thermal insulation by snow flattens the T_g gradient (−0.25°C/100 m; Figure 6g) compared to that of T_a (−0.38°C/100 m; Figure 6c). Because the study area in Valais is a very sunny region (MeteoSwiss 2020b) according to its inner Alpine climate, the above-described effect of radiation is probably more pronounced than in other alpine regions.

The reason why the T_a gradient is flatter in winter than in summer (Figures 6c, 6d) can be found in cold air pools (CAPs), which have been observed in mountains around the world; for example, by the Mount Washington Observatory (2019), in the Spanish Pyrenees (Conangla et al. 2018), and in the Swiss Jura Mountains (Vitasse et al. 2017). According to these studies, CAPs frequently form on clear winter nights with little air turbulence (i.e., calm winds): The strong longwave outgoing radiation efficiently cools the ground surface, which cools down the near-surface air above. The near-surface air thus becomes denser than the air above and flows downslope, called katabatic wind. This cold air fills the valley and leads to a CAP. This mechanism leads to a positive elevational T_a gradient called inversion. Because inversions occur frequently on winter nights and may persist throughout the day (Zhong et al. 2001), the mean T_a gradient in winter is clearly lower than that in summer.

In winter, not only the elevational T_a gradient is flatter than in summer (Figures 6c, 6d), but also the elevational T_g gradient (Figures 6g, 6h). In addition to the effect of thermal insulation by snow increasing with elevation, winterly CAP formation flattens the T_g gradient: CAP can efficiently cool the ground on the lower slope where the snow cover is less deep and lasts shorter than higher up. Moreover, CAP inversions are often associated with fog, which can persist throughout the day (Zhong et al. 2001). This reduces incoming as well as outgoing radiation. Because incoming radiation contributes much more to the ground heat balance than outgoing radiation (Häckel 2016), the CAP-induced fog leads to further ground cooling on the lower slope, flattening the T_g gradient in winter. Consequently, upslope increasing radiation flattens the T_g gradient in summer less than CAP and insulation by snow together in winter.

The subdaily T_g amplitude remains roughly constant with elevation in summer; that is, from June to August (Figure 6h). In winter—that is, from December to February—it strongly decreases upslope (Figure 6g), which can be attributed to the thermal insulation of the snow cover increasing upslope. Averaged over the year, the subdaily T_g amplitude slightly decreases with elevation (Figure 6b), which is typical for arid mountains such as the Valais (Richter 1996). The subdaily T_g amplitude deviates the most from that of T_a in winter (Figures 6c, 6d, 6g, 6h), indicating that snow is likely responsible for this. Above about 2,000 m a.s.l., T_g no longer shows subdaily fluctuations (Figure 6g). This is consistent with Figure 5, showing that the temporal gaps in the snow cover period for the S slope in the field from December to February decrease upslope and disappear above 2,000 m a.s.l.

However, not only in winter but also in summer without snow, the subdaily amplitude is still smaller in the ground than in the air except above about 2,500 m a.s.l. (Figures 6h, 6d). This is probably due to the much higher specific heat capacity of ground compared to air; that is, for a given temperature change, much more specific heat energy has to be taken up or released in the ground compared to air. The subdaily T_g amplitude does not

decrease upslope as for T_a. This finding is in strong contrast to Richter (1996). He suggests that the subdaily T_a amplitude is much lower than that at the ground surface for both humid and arid mountains because the ground surface is heated by incoming radiation in the daytime and cooled by outgoing radiation at night. However, in this study, the subdaily T_g amplitude was much lower than that in the air due to the snow cover in winter and the higher specific heat capacity of ground compared to air in summer. These two effects together must thus overcompensate for the radiative effect on the subdaily T_g amplitude described by Richter (1996).

The seasonal temperature amplitudes decrease with elevation for both air and ground but much more for ground (Figures 6c, 6d, 6g, 6h). This is probably due to the snow cover lasting longer (Figure 6i) and becoming deeper upslope, leading to reflection of the major part of the incoming radiation, to prevention of outgoing radiation from the ground surface, and to efficient insulation of the ground against cooling in winter and against warming until early summer.

The dependence of air ice days (ID_a) and air frost change days (FCD_a) on elevation (Figures 6e, 6f) can be explained by the elevational dependence of the subdaily T_a amplitudes. FCD_a first increases with elevation because the probability for T_a in winter nights to be negative increases upslope, whereas T_a in winter during daytime mostly reaches positive values; that is, ID_a is quite low. However, after reaching a local maximum at about 1,900 m a.s.l., FCD_a decreases upslope as T_a on winter nights but also during the daytime becomes negative more often; that is, ID_a exponentially increases. A local FCD_a maximum was reported by Rodler (1885) for the upper Rhine valley and by Fritz (1976) for the Eastern Alps between 1,400 and 1,700 m a.s.l. The higher value in this study is probably due to the dryer inner Alpine climate.

In contrast to FCD_a, the number of ground frost change days (FCD_g) close to zero over the observed elevational range (Figure 6f) implies that T_g is mostly either ≥0°C or ≤0°C throughout the day. This behavior can be explained by thermal buffering of T_g due to the coexistence of water and ice (i.e., zero curtain) when T_a can be negative at night but positive during the day.

The number of ground ice days (ID_g) is higher than ID_a (Figure 6e) because once the mean daily T_g drops below 0°C, all days in the following frost period are ground ice days until all of the thermally buffered ground ice has thawed in spring. Furthermore, compared to air, ground has a far higher specific heat capacity, making it thermally more inertial.

The first ground freezing day ($FD1_g$) occurs only slightly earlier upslope (Figure 6k), although the yearly mean of T_g markedly decreases with elevation (Figure 6a). Thus, there must be a distinct rapid T_a drop in autumn or early winter initiating near-surface ground frost throughout the slope instantaneously.

The first ground thawing day ($TD1_g$; Figure 6k) correlates well with the first snow-free day (SFD1; Figure 6j). In fact, at most of the observed elevations, $TD1_g$ and SFD1 are identical; that is, T_g exceeds 0°C for the first time after winter on the same day when the snow cover disappears (case 1). However, at 908, 1,508, 1808, and 1,958 m a.s.l., $TD1_g$ occurred earlier than SFD1; that is, the ground could thaw only 5 cm below the snow cover base, which must have not more than 0°C (case 2). In case 1, the ground frost is thawed by both the geothermal heat flux upwards ($q_\uparrow$) and the atmospheric heating downwards ($q_\downarrow$). In case 2, the ground frost can only be degraded by $q_\uparrow$.

The upslope diverging regression lines for the maximum and minimum of the ground temperature/depth gradient (T_g/z) in summer mean that the heat gain of the ground surface by day and the heat loss at night both increase with elevation (Figure 6n). This can be ascribed to radiation: As the atmosphere gets thinner with elevation, the incoming radiation by day and the outgoing radiation at night become stronger upslope.

The upslope converging regression lines for the T_g/z maximum and minimum in winter with values below 0°C/m at 700 m a.s.l. mean that the ground is losing heat to the atmosphere not only at night but also during the day over the whole elevational range observed (Figure 6m). However, the difference between day and night becomes progressively smaller upslope, which is attributable to the thermal insulation of the snow cover increasing upslope. As the regression lines for the yearly mean of T_g/z converge upslope (Figure 6l), the winter "snow effect" overbalances the summer "radiation effect" for the whole year.

Elevational thermal gradients—Separated by slope aspect

A possible reason for the effect of slope aspect on the yearly mean T_a (on the field), even though it is quite weak (Figure 7a), is the balancing air fluxes between the N and S slopes. The flatter elevational T_a gradient on the N slope than on the S slope over the year (Figure 7a) might be due to more frequent and stronger katabatic winds on the N slope due to cooler air, resulting in a T_a decrease at the lower slope.

The higher yearly means of T_g (under forest) and its moderately steeper elevational gradient on the S slope (Figure 7b) result from the strong N–S differences in T_g in winter (Figures 7c, 7g) and are in accordance with Mani (1962) and Barry and Van Wie (1974). In winter, the sun's incidence angle is quite low, so the ground, if

bare of snow, can be irradiated from the side underneath the canopy. Because snow-free ground is more likely on the S slope and at lower elevations (Figures 5, 7k, 7l), the aspect-related difference in radiation reaching the ground becomes relevant and decreases upslope (even more on the N slope) with the more frequent and deeper snow cover. In summer, T_g becomes slightly higher on the N slope toward the tree line (Figures 7d, 7h). This means that the shading of the ground by the forest canopy is stronger on the S slope, which is probably due to a denser canopy there caused by higher radiation favoring photosynthesis. The subdaily T_g variation is lower on the N slope than on the S slope, lower in winter than in summer, and lower at 2,100 m a.s.l. than at 700 m a.s.l. (Figures 7c, 7g, 7d, 7h). These findings suggest that snow cover decreases subdaily T_g variations by thermal insulation. This effect is the stronger the longer the ground is covered by snow and the deeper the snow cover is.

The aspect-related differences concerning the number of ice days in the air (ID_a) are marginal (Figure 7e) and suggest air convection across the valley bottom as the reason, as argued for T_a above. Regarding the number of frost change days in the air (FCD_a), a sigmoid curve is predefined and fitted to data for the N and S slopes (Figure 7f), because this type of curve was found for FCD_a in Figure 6f already. Because ID_a is roughly equal for N and S slopes, the higher FCD_a values on the N slope mean that frost changes occur on the N slope on days when T_a on the S slope is positive throughout the day. These conditions prevail, for example, at 1,958 m a.s.l. in November, with 11 FCD_a on the N slope but 0 FCD_a on the S slope and no ID_a for both aspects. Extrapolating the FCD_a curve for the N slope upslope would result in a local maximum of 174 FCD_a at about 2,150 m a.s.l.; that is, higher than the maximum on the S slope. This seems to be illogical at first glance because FCD_a decreases in favor of ID_a above the local maximum of FCD_a on the S slope but FCD_a still increases on the N slope. However, ID_a is slightly higher on the N slope and increases above the elevation of the local maximum on the S slope but not at the expense of FCD_a. This is possible because FCD_a mainly occur in spring and autumn but ID_a occur mainly in winter.

Up to about 1,800 m a.s.l., the higher number of ground ice days (ID_g) on the N slope compared to the S slope (Figure 7i) can be explained by the aspect-related differences in radiation, which become stronger downslope because the N slope gets also less scatter radiation toward the valley. Surprisingly, above 1,800 m a.s.l., there are more ID_g on the S slope. This elevation is roughly the 0°C line for T_g in winter on the S slope (Figures 7c, 7g). According to Figure 5, the snow cover at 1,958 m a.s.l. begins later on the S slope and is often interrupted in autumn/early winter compared to the N slope. That means that the ground on the S slope above 1,800 m a.s.l. is less often and to a lesser degree thermally protected by snow from the cold atmosphere than the N slope, resulting in more ID_g on the S slope. Nevertheless, T_g can be lower on the N slope than on the S slope on average in winter and over the year. FCD_g is much lower than FCD_a not only on the S slope but also on the N slope (Figure 7j).

Elevational thermal gradients—Separated by land cover

The thermally equalizing effect of air convection between field and forest is also visible in the yearly aggregated data for T_a and its elevational gradient: These values differ only marginally (Figure 8a). Under forest, shading by the canopy leads to less radiative ground heating and thus lower T_g values (Figure 8b). As radiation increases with elevation, so does the T_g difference between field and forest, resulting in a steeper elevational T_g gradient under forest in summer (Figures 8d, 8h) and averaged over the year (Figure 8b). In winter during the daytime, T_g is lower under forest (Figure 8c) due to the shallower snow depth caused by interception. Because snow cover is less frequent toward lower elevations, this difference reduces downslope. In winter nights, T_g values under forest are higher than those for field on the lower slope (Figure 8g) because the canopy reduces the nocturnal longwave outgoing radiation, thus decreasing ground cooling. Because the snow cover is shallower and less frequent on the lower slope, outgoing radiation is crucial here. Inversely, the snow cover in winter increases upslope and so the difference due to interception becomes increasingly relevant. Consequently, T_g under forest at night increasingly falls behind T_g in the field (Figure 8g). Thus, not only in summer but also in winter the T_g gradient is steeper for forest than for field (Figure 8g). The intersection of the regression lines in Figure 8g explains why the subdaily T_g amplitude in winter is higher in the field on the lower slope but higher in the forest on the upper slope (Figures 8c, 8g). In summer, the subdaily T_g amplitude is much lower under forest (Figures 8d, 8h) due to its thermal damping effect caused by radiation shielding. Comparing Figure 8c to Figure 8d and Figure 8g to Figure 8h reveals that forest also dampens seasonal T_g variations compared to field.

Regarding the number of air ice days (ID_a), the values are higher for forest than field (Figure 8e); regarding the number of air frost change days (FCD_a) the reverse is found (Figure 8f). The differences regarding ID_a can be ascribed to the reduction of radiation by the canopy and the thinner snow cover due to interception. Forest reduces FCD_a compared to field; that is, it stabilizes either frost or frost-free conditions of the

air throughout a day by reducing the incoming as well as outgoing radiation compared to the field. Thus, forest thermally dampens the subdaily atmospheric variability. The sigmoid course of FCD_a with elevation is also valid for forest.

Ground ice days (ID_g) are less frequent under forest than in the field up to 1,300 m a.s.l. (Figure 8i). The reason is the sun's low incidence angle in winter when ice days occur: During the daytime, a high portion of solar radiation reaches the inclined ground (if free of snow) even under forest, so the forest's deficit in incoming radiation compared to the field is small. This deficit is overcompensated at night when the forest protects a snow-free ground from cooling. Above 1,300 m a.s.l., the higher ID_a under forest is due to snow interception weakening thermal insulation. The independence of ID_g from elevation in the field suggests that the effect of the elevational T_g decrease appears just to balance the insulating effect of the growing snow cover. Figure 8j shows that the number of ground frost change days (FCD_g) is also marginal under forest compared to FCD_a and that the ice–water buffer in the ground also applies for forest.

Conclusions and implications

Thermal parameters were investigated as a function of elevation as a main factor and slope aspect (north vs. south) and land cover (open field vs. forest) as covariables in this study. Assuming the observed but not measured processes that incoming solar radiation heats up the ground, CAPs favor the formation of fog, and a forest canopy intercepts snow, the following conclusions can be drawn:

- Annual mean ground temperatures (T_g) are some degrees Celsius higher and their average elevational gradient is flatter than that for air because radiative ground heating in summer and thermal protection of the ground from atmosphere in winter both increase with elevation.
- The elevational air temperature gradient is flatter in winter than summer due to CAPs in the valleys. This gradient is also flatter in winter than in summer because of two effects: (1) on lower slopes, radiation is reduced due to CAP-induced fog and (2) on higher slopes, the ground is thermally insulated from the cold atmosphere by snow.
- In contrast to Richter (1996), we found subdaily T_g amplitudes to be strongly damped compared to the atmosphere and to decrease with elevation. This indicates the importance of thermal insulation by snow in addition to radiation.
- In contrast to the atmosphere, there is no distinct maximum of frost change days in the ground (FCD_g) and their number is marginal. This can be explained by the thermal buffering of the ground against the atmosphere because water and ice coexist in the ground and stabilize T_g at 0°C due to latent heat exchange.
- The elevational T_g gradient under forest is flatter on the N slope than on the S slope. The difference is highest in winter because the aspect-related difference in radiation reaching the ground becomes relevant in the snow-free valley and decreases upslope (even more on the N slope) due to increasing insulation by snow.
- Surprisingly, above 1,800 m a.s.l. there are more ground ice days (ID_g) on the S slope than on the N slope under forest. This can be attributed to a longer and thicker snow cover on the N slope above 1,800 m a.s.l. thermally insulating the ground from the colder atmosphere.
- Forest reduces the annual mean T_g compared to open field due to shading by the canopy and damps subdaily T_g variations by reducing incoming radiation during the daytime and outgoing radiation at night.
- Under forest, snow interception in winter reduces the thermal insulation by snow and thus T_g.

To sum up, the research questions introduced in this study can be answered as follows:

- Temperatures and related thermal parameters in mountains differ considerably between air and near-surface ground and depend on elevation differently regarding subdaily and seasonal amplitudes.
- Compared to air, the dependence of the thermal regime on elevation is attenuated in the ground, and this effect is stronger on the N slope than on the S slope and stronger for forest than field.
- The investigated environmental factors elevation, aspect, and land cover integrate various physical basic factors that change in complex ways at once. In this study, radiation, snow cover, and ground heat transfer are interpreted as most relevant basic factors ultimately controlling the ground thermal regime in contrast to air.

Compared to the meteorological standard values (1981–2010) of Montana (MeteoSwiss 2016a) at a middle elevation of the study site, the year of this study was average with regard to air temperature and

sunshine hours (both 3 percent over standard), below average with regard to fresh snow as well as ice and frost change days in the air (46, 28, and 15 percent under standard, respectively), and above average with regard to precipitation (24 percent over standard). Thus, for climate standard conditions, the thermally damping effect of snow would probably be stronger and that of phase changes probably weaker. However, the two effects' alterations in the study year compared to standard conditions countered each other. Further measurements might help to detect long-term changes in these relationships.

The findings of this study apply most exactly for moderately continental alpine regions in the temperate zone such as Valais. However, the principles and mechanisms controlling the ground thermal regime and elevational gradients, in contrast to those of air, can be transferred to other mountains in the world. Depending on a region's climate, it can be determined which of this study's factors are relevant and to what extent. The knowledge gained in this study helps to better understand ecosystems, agriculture, and forestry in mountain regions because a large portion of the living biomass is underground and is strongly affected by the ground thermal regime.

Acknowledgments

This research did not receive any specific grant from funding agencies. We thank Marcia Philipps (WSL Institute for Snow and Avalanche Research SLF, Davos, Switzerland) and the reviewers of *AAAR* for their valuable review of the article.

Disclosure statement

The authors declare that they have no competing interests.

ORCID

Armin Rist http://orcid.org/0000-0002-2935-4051
Lotti Roth http://orcid.org/0000-0001-9979-3909

References

Ashcroft, M. B., and J. R. Gollan. 2013. Moisture, thermal inertia, and the spatial distributions of near-surface soil and air temperatures: Understanding factors that promote microrefugia. *Agricultural and Forest Meteorology* 176:77–89. doi:10.1016/j.agrformet.2013.03.008.

Aulitsky, H. 1962. Die Bodentemperaturverhältnisse einer zentralalpinen Hochgebirgs-Hangstation II. *Archiv für Meteorologie, Geophysik und Bioklimatologie* B, 11:301–62.

Barry, R. G. 2008. *Mountain weather and climate*. Cambridge: Cambridge University Press.

Barry, R. G., and C. C. Van Wie. 1974. Topo- and microclimatology in alpine areas. In *Arctic and alpine environments*, ed. J. D. Ives and R. G. Barry, 73–83. London: Methuen.

Bertoldi, G., C. Notarnicola, G. Leitinger, S. Endrizzi, M. Zebisch, S. Della Chiesa, and U. Tappeiner. 2010. Topographical and ecohydrological controls on land surface temperature in an alpine catchment. *Ecohydrology* 3 (2):189–204. doi:10.1002/eco.129.

Blüthgen, J. 1980. *Allgemeine Klimageographie*. Berlin: de Gruyter.

Bouet, M. 1978. Le Valais. In *Klimatologie der Schweiz*, Series ed. S. M. Zentralanstalt, (Regionale Klimabeschreibung ed., 88–114). Zürich: Schweizerische Meteorologische Zentralanstalt.

Camenzind, R., A. Stalder, A. Finger, P. Kläy, P. Wisler, and U. Wittwer. 2011. *Landschaftstypologie Schweiz*. (Federal Office for Spatial Development, Federal Office for the Environment, & Federal Statistical Office Eds.). Bern: Federal Office for Spatial Development.

Conangla, L., J. Cuxart, M. A. Jimenez, D. Martinez-Villagrasa, J. R. Miro, D. Tabarelli, and D. Zardi. 2018. Cold-air pool evolution in a wide Pyrenean valley. *International Journal of Climatology* 38 (6):2852–65. doi:10.1002/joc.5467.

Coppernoll-Houston, D., and C. Potter. 2018. Field measurements and satellite remote sensing of daily soil surface temperature variations in the Lower Colorado Desert of California. *Climate* 6 (4):11. doi:10.3390/cli6040094.

Cordova, M., R. Celleri, C. J. Shellito, J. Orellana-Alvear, A. Abril, and G. Carrillo-Rojas. 2016. Near-surface air temperature lapse rate over complex terrain in the Southern Ecuadorian Andes: Implications for temperature mapping. *Arctic, Antarctic, and Alpine Research* 48 (4):673–84. doi:10.1657/aaar0015-077.

Fries, A., R. Rollenbeck, D. Gottlicher, T. Nauss, J. Homeier, T. Peters, and J. Bendix. 2009. Thermal structure of a megadiverse Andean mountain ecosystem in southern Ecuador and its regionalization. *Erdkunde* 63 (4):321–35. doi:10.3112/erdkunde.2009.04.03.

Fritz, P. 1976. Gesteinsbedingte Standorts-und Formen-Differenzierung rezenter Periglazialerscheinungen in den Ostalpen. *Mitteilungen der Österreichischen Geographischen Gesellschaft* 118 (1):237–73.

Google. n.d. European Alps, Terrain [Website]. https://www.google.ch/maps/@45.7970486,8.349896,7z/data=!5m1!1e4

Graae, B. J., P. De Frenne, A. Kolb, J. Brunet, O. Chabrerie, K. Verheyen, N. Pepin, T. Heinken, M. Zobel, and A. Shevtsova. 2012. On the use of weather data in ecological studies along altitudinal and latitudinal gradients. *Oikos* 121 (1):3–19. doi:10.1111/j.1600-0706.2011.19694.x.

Grunow, J. 1952. Beiträge zum Hangklima. *Berichte des Deutschen Wetterdienstes der US-Zone* 8 (35):293–98.

Gutersohn, H. 1961. *Alpen*. Vol. 2. Bern: Kümmerly + Frey.

Haberkorn, A., N. Wever, M. Hoelzle, M. Phillips, R. Kenner, M. Bavay, and M. Lehning. 2017. Distributed snow and rock temperature modelling in steep rock walls using Alpine3D. *The Cryosphere* 11 (1):585–607. doi:10.5194/tc-11-585-2017.

Häckel, H. 2016. *Meteorologie*. Stuttgart: Ulmer.

Hanson, S., and M. Hoelzle. 2004. The thermal regime of the active layer at the Murtèl rock glacier based on data from

2002. *Permafrost and Periglacial Processes* 15 (3):273–82. doi:10.1002/ppp.499.

Happoldt, H., and L. Schrott. 1989. Globalstrahlung und Bodentemperaturen in der periglazialen Höhenstufe am Aconcagua, argentinische Hochanden. In *Bayreuther geowissenschaftliche Arbeiten, Vol. 14, Beiträge zur Geomorphologie: Quartärmorphologie, Relief Tektonik*, ed. K. Hüser, 35–45. Bayreuth: Naturwissenschaftliche Gesellschaft Bayreuth.

Hillel, D. 2004. *Introduction to environmental soil physics*. Burlington: Elsevier.

Kirchner, M., T. Faus-Kessler, G. Jakobi, M. Leuchner, L. Ries, H. E. Scheel, and P. Suppan. 2013. Altitudinal temperature lapse rates in an Alpine valley: Trends and the influence of season and weather patterns. *International Journal of Climatology* 33 (3):539–55. doi:10.1002/joc.3444.

Körner, C. 2003. *Alpine plant life: Functional plant ecology of high mountain ecosystems*. 2nd ed. Berlin: Springer.

Lehmkuhl, F., and M. Klinge. 2000. Bodentemperaturmessungen aus dem Mongolischen Altai als Indikatoren für periglaziale Geomorphodynamik in hochkontinentalen Gebirgsräumen. *Zeitschrift für Geomorphologie* 44 (1):75–102.

Löffler, J. 2007. The influence of micro-climate, snow cover, and soil moisture on ecosystem functioning in high mountains. *Journal of Geographical Sciences* 17 (1):3–19. doi:10.1007/s11442-007-0003-3.

Mani, M. S. 1962. *Introduction to high elevation entomology; insect life above the timber-line in the North-West Himalaya*. London: Methuen.

Matsuoka, N. 2001. Solifluction rates, processes and landforms: A global review. *Earth-Science Reviews* 55(1–2):107–34. doi:10.1016/S0012-8252(01)00057-5.

Matsuoka, N., K. Hirakawa, T. Watanabe, and K. Moriwaki. 1997. Monitoring of periglacial slope processes in the Swiss Alps: The first two years of frost shattering, heave and creep. *Permafrost and Periglacial Processes* 8 (2):155–77. doi:10.1002/()1099-1530.

Maurer, J. 1916. Bodentemperatur und Sonnenstrahlung in den Schweizer Alpen. *Meteorologische Zeitschrift* 33:193–99.

MeteoSwiss. 2016a. *Climate norm values, climsheet Montana*. Zürich-Flughafen: Federal Office of Meteorology and Climatology MeteoSwiss.

MeteoSwiss. 2016b. *Climate norm values, climsheet Sion, Montana*. Zürich-Flughafen: Federal Office of Meteorology and Climatology MeteoSwiss.

MeteoSwiss. 2017a. Meteorological archive data of the ground based measuring net of MeteoSwiss IDAWEB. https://gate.meteoswiss.ch/idaweb.

MeteoSwiss. 2017b. Norm values 1981–2010: Sum of precipitation. (pp. Normwerte 1981–2010: Niederschlagssummen; Meteostationen von MeteoSchweiz), Federal Office of Meteorology and Climatology MeteoSwiss, Zürich-Flughafen.

MeteoSwiss. 2020a. Mean yearly precipitation (mm) 1981–2010. https://www.meteoswiss.admin.ch/home/climate/swiss-climate-in-detail/climate-normals/norm-value-charts.html?filters=precip_8110_yy

MeteoSwiss. 2020b. Mean yearly relative sunshine duration 1981–2010. https://www.meteoswiss.admin.ch/home/climate/swiss-climate-in-detail/climate-normals/norm-value-charts.html?filters=precip_8110_yy.

Minder, J. R., P. W. Mote, and J. D. Lundquist. 2010. Surface temperature lapse rates over complex terrain: Lessons from the Cascade Mountains. *Journal of Geophysical Research* 115 (D14):13. doi:10.1029/2009jd013493.

Mount Washington Observatory. 2019. Cold-air pools in mountain valleys [Website]. Accessed November 24, 2019. https://www.mountwashington.org/research-and-product-testing/current-projects/cold-air-pools-in-mountain-valleys.aspx.

Müller, H., and C. D. Whiteman. 1988. Breakup of a nocturnal temperature inversion in the Dischma Valley during DISKUS. *Journal of Applied Meteorology* 27 (2):188–94. doi:10.1175/1520-0450(1988)027<0188:boanti>2.0.co;2.

Navarro-Serrano, F., J. I. Lopez-Moreno, C. Azorin-Molina, E. Alonso-Gonzalez, M. Tomas-Burguera, A. Sanmiguel-Vallelado, J. Revuelto, and S. M. Vicente-Serrano. 2018. Estimation of near-surface air temperature lapse rates over continental Spain and its mountain areas. *International Journal of Climatology* 38 (8):3233–49. doi:10.1002/joc.5497.

Pepin, N. 2001. Lapse rate changes in northern England. *Theoretical and Applied Climatology* 68 (1–2):1–16. doi:10.1007/s007040170049.

Richter, M. 1996. Klimatologische und pflanzenmorphologische Vertikalgradienten in Hochgebirgen. *Erdkunde* 50 (3):205–37. doi:10.3112/Erdkunde.

Rist, A. 2007. Hydrothermal processes within the active layer above alpine permafrost in steep scree slopes and their influence on slope stability. (Dissertation, University of Zürich), Zürich.

Rodler, A. 1885. Die vertikale Verteilung der Temperaturs-chwankungen um den Frostpunkt in der Schweiz. *Zeitschrift der Österreichischen Gesellschaft für Meteorologie* 20:4–17.

Rolland, C. 2003. Spatial and seasonal variations of air temperature lapse rates in Alpine regions. *Journal of Climate* 16 (7):1032–46. doi:10.1175/1520-0442(2003)016<1032:sasvoa>2.0.co;2.

Swisstopo. 2018. DHM25 Hillshade. https://map.geo.admin.ch/?lang=en&zoom=4&topic=ech&bgLayer=ch.swisstopo.pixelkarte-farbe&layers=ch.swisstopo.zeitreihen,ch.bfs.gebaeude_wohnungs_register,ch.bav.haltestellen-oev,ch.swisstopo.swisstlm3d-wanderwege,ch.swisstopo.digitales-hoehenmodell_25_reliefschattierung&layers_opacity=1,1,1,0.8,1&layers_visibility=false,false,false,false,true&layers_timestamp=18641231,,,,&E=2601563.85&N=1124510.30.

Tang, Z. Y., and J. Y. Fang. 2006. Temperature variation along the northern and southern slopes of Mt. Taibai, China. *Agricultural and Forest Meteorology* 139 (3–4):200–07. doi:10.1016/j.agrformet.2006.07.001.

Turner, H, P. Rochat, and A. Streule. 1975. Thermische Charakteristik von Hauptstandortstypen im Bereich der oberen Waldgrenze (Stillberg, Dischmatal bei Davos). *Mitteilungen Eidgenössische Anstalt für das Forstliche Versuchswesen* 51:95–119.

Veit, H. 2002. *Die Alpen: Geoökologie und Landschaftsentwicklung*. Stuttgart: Verlag Eugen Ulmer.

Vitasse, Y., G. Klein, J. W. Kirchner, and M. Rebetez. 2017. Intensity, frequency and spatial configuration of winter temperature inversions in the closed La Brevine valley, Switzerland. *Theoretical and Applied Climatology* 130 (3–4):1073–83. doi:10.1007/s00704-016-1944-1.

Zenklusen Mutter, E., J. Blanchet, and M. Phillips. 2010. Analysis of ground temperature trends in Alpine permafrost using generalized least squares. *Journal of Geophysical Research* 115 (F4):F04009. doi:10.1029/2009jf001648.

Zhang, T., R. L. Armstrong, and J. Smith. 2003. Investigation of the near-surface soil freeze-thaw cycle in the contiguous United States: Algorithm development and validation. *Journal of Geophysical Research: Atmospheres* 108 (D22):14. doi:10.1029/2003jd003530.

Zhong, S. Y., C. D. Whiteman, X. D. Bian, W. J. Shaw, and J. M. Hubbe. 2001. Meterological processes affecting the evolution of a wintertime cold air pool in the Columbia Basin. *Monthly Weather Review* 129 (10):2600–13. doi:10.1175/1520-0493(2001)129<2600:mpateo>2.0.co;2.